Biomaterials Science

ROYAL SOCIETY OF CHEMISTRY

PAPER

View Article Online
View Journal | View Issue

Cite this: *Biomater. Sci.*, 2025, **13**, 5202

Polyaspartamide-based antimicrobials for combatting bacterial infections

Wenlong Zhang,[a,b] Guowenlie Gao,[a,b] Yuqian Ji,[a,b] Mingming Zhao,[a,b] Pengqi Wan,*[a] Chunsheng Xiao *[a,b] and Xuesi Chen *[a,b]

The increasing challenge of antimicrobial resistance has stimulated research on antibacterial polymers, which offer enhanced therapeutic potential due to their facile synthesis, low immunogenicity, and superior stability compared to natural antimicrobial peptides. Herein, a series of cationic polyaspartamides ($PASP_nDA_m$) with different side chain lengths (*m*) and degrees of polymerization (*n*) were synthesized through ammonolysis reaction of poly(β-benzyl-L-aspartate) (PBLA) to systematically investigate their antibacterial activity and biocompatibility. All $PASP_nDA_m$ exhibited antibacterial activity. Among the $PASP_nDA_m$, $PASP_{10}DA_6$ (degree of polymerization of 10, bearing side chains modified with 1,6-hexamethylenediamine) displayed potent activities against bacteria (*S. aureus* and *E. coli*, MIC = 7.8 μg mL^{-1}) and had the highest selectivity index of 96. Further mechanistic study revealed that $PASP_{10}DA_6$ killed bacteria by disrupting the integrity of the bacterial membrane, thereby leading to bacterial death. Based on this unique bactericidal mechanism, $PASP_{10}DA_6$ showed fast bacterial killing kinetics and was less likely to induce bacterial resistance for up to 15 generations. In a mouse skin bacterial infection model, $PASP_{10}DA_6$ showed effective *in vivo* antibacterial activity and negligible toxicity. Hence, this study provides a promising strategy for treating clinical bacterial infections.

Received 30th June 2025,
Accepted 3rd August 2025

DOI: 10.1039/d5bm00994d

rsc.li/biomaterials-science

1. Introduction

The discovery of penicillin by Alexander Fleming in 1928 marked the beginning of the antibiotic era, revolutionizing the treatment of previously fatal diseases.[1,2] However, the widespread use of antibiotics has created a significant challenge in the form of antimicrobial resistance (AMR). The emergence and evolution of AMR represent a grave challenge to public health, fueled by the selective pressure exerted by antibiotic exposure.[3] Over time, bacteria have evolved diverse mechanisms to resist the effects of antibiotics, including enzymatic degradation, activation of efflux pumps, and genetic mutations that confer resistance.[4,5] The ongoing arms race between microbes and antibiotics has led to the emergence of multidrug-resistant pathogens, rendering conventional antibiotics ineffective and threatening the efficacy of contemporary medical therapies.[6,7] In this post-antibiotic era, characterized by a paucity of treatment alternatives and the resurgence of infections previously under control, the development of novel antimicrobial approaches has become an urgent necessity.

Natural antimicrobial peptides (AMPs) are small cationic molecules produced by various organisms as part of their innate immune system, playing a crucial role in defending against a wide range of pathogens.[8] AMPs have garnered significant attention for their potent antimicrobial activity and unique mechanisms of action.[9] However, their practical application is hindered by high production costs, physiological instability and potential cytotoxicity.[10,11] Antibacterial poly(amino acids) offers a cost-effective and scalable solution that mimics the membrane-disruptive mechanisms of AMPs[12–15] while overcoming AMPs' limitations through tunable molecular structures that enhance stability and improve efficacy.[16] Polyaspartamides, a class of biocompatible and biodegradable polymers derived from aspartic acid, have found widespread applications in fields including drug delivery and tissue engineering owing to their versatile properties.[17,18] Research on antimicrobial polyaspartamides began in 1966, when "α,β-poly-DL-aspartic acid 3-aminopropylamide" was prepared from polysuccinimide (PSI) through aminolysis with 1,3-propanediamine. These polyaspartamides showed notable antimicrobial activity against *Cryptococcus neoformans*, *Histoplasma capsulatum*, *Staphylococcus aureus*, and *Mycobacterium smegmatis*.[19,20] However, to date, research on antibacterial polyaspartamides

[a]*State Key Laboratory of Polymer Science and Technology, Key Laboratory of Polymer Ecomaterials, Changchun Institute of Applied Chemistry, Chinese Academy of Sciences, Changchun 130022, P. R. China. E-mail: wpengqi@ciac.ac.cn*
[b]*School of Applied Chemistry and Engineering, University of Science and Technology of China, Hefei 230026, P. R. China. E-mail: xiaocs@ciac.ac.cn, xschen@ciac.ac.cn*

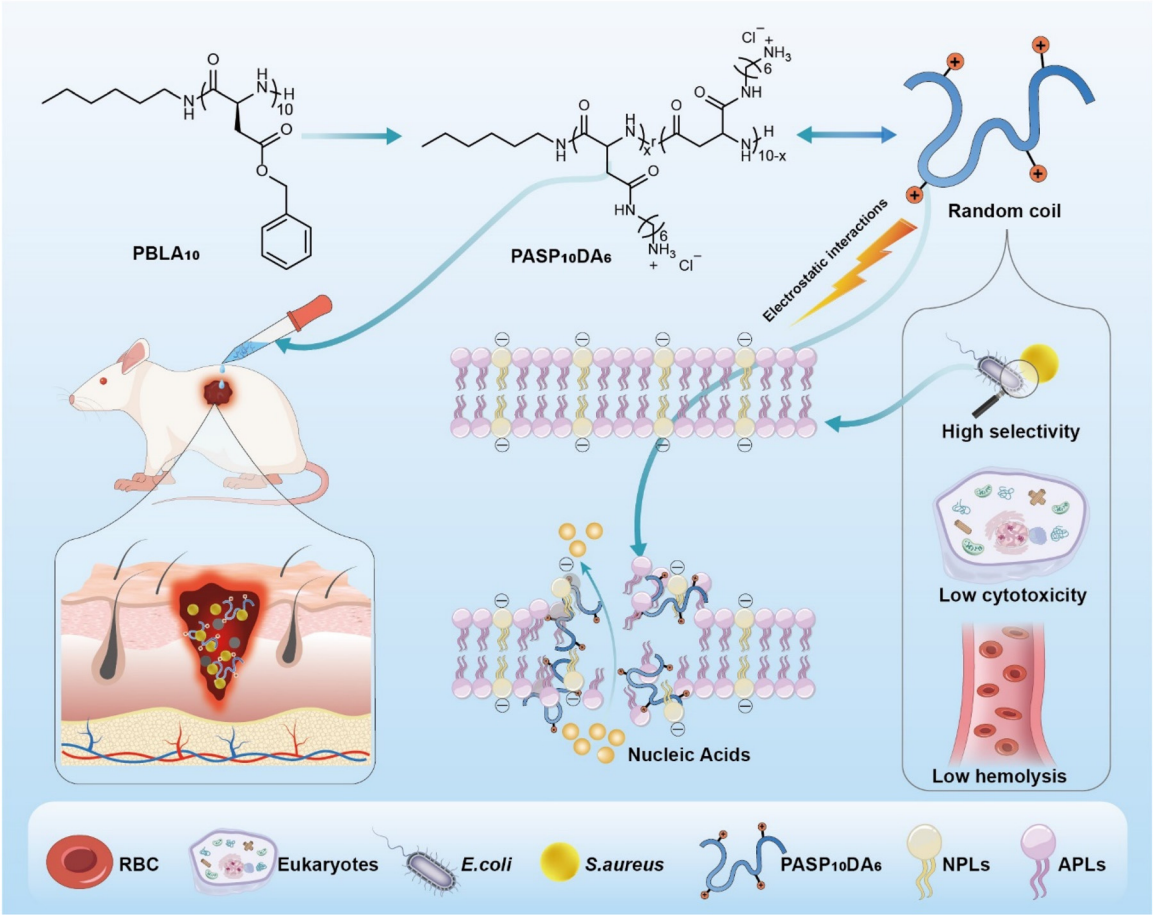

Scheme 1 Schematic of the synthesis of $PASP_{10}DA_6$ for the treatment of *S. aureus* infection in mouse epidermis.

remains relatively scarce and is primarily confined to the effects of specific degrees of polymerization (DPs)[21–26] and side chain structures[27] on their antibacterial performance, lacking effective screening of different DPs and side chain structures as well as systematic studies on the structure–activity relationships between these structural parameters[28] and antibacterial activity. Such screening and in-depth exploration of structure–activity relationships are essential for guiding the rational design and performance optimization of antibacterial polyaspartamides.

In this study, we conducted a thorough investigation into the influence of the DP and side chain length on the antimicrobial activity and biocompatibility of $PASP_nDA_m$ obtained from the aminolysis of PBLA with different diamines (n denotes the DP of polymer, and m denotes the number of carbon atoms located between two amino groups in the diamines). Based on the screening tests, $PASP_{10}DA_6$ had better antibacterial efficacy and biocompatibility compared to the other tested polyaspartamides. $PASP_{10}DA_6$ exerted its bactericidal effect through membrane disruption. Furthermore, in a bacterial infection model on mouse epidermis, $PASP_{10}DA_6$ demonstrated superior therapeutic performance compared to conventional antibiotics, highlighting its potential as an effective antimicrobial agent (Scheme 1).

2. Experimental section

2.1. Synthesis of $PASP_nDA_m$

The aminolysis reaction was performed following a modified literature procedure.[27] $PBLA_{10}$ (200 mg, 0.095 mmol) was dissolved in anhydrous DMSO (10 mL) in a flame-dried flask under a nitrogen atmosphere. Ethylene diamine (50 eq. excess of benzyl ester units) was added, and the reaction mixture was stirred at room temperature for 1 h. After 1 h, the aminolyzed product was precipitated into an excess of cold diethyl ether (100 mL). The precipitate was collected by centrifugation (10 000 rpm, 10 min) and washed with cold ether (20 mL) to remove residual ethylene diamine and solvent. The aminolyzed polymer was dissolved in deionized water (5 mL) and transferred to a pre-treated dialysis tube (MWCO 200 Da). Dialysis was conducted against HCl solution (0.01 M, pH = 1.0) at room temperature with six changes of the dialysis medium over 48 h. The dialyzed polymer solution was lyophilized to yield the final product, $PASP_{10}DA_2$, as an off-white fluffy solid (85 mg). Additionally, aminolysis of PBLA samples with different DPs (20, 30, and 40) and different diamines (1,3-propanediamine, 1,4-butanediamine, 1,5-pentanediamine, and 1,6-hexanediamine) was conducted using the same method.

2.2. Minimum inhibitory concentration (MIC) assay

The MICs of $PASP_nDA_m$ against *S. aureus* and *E. coli* were evaluated using the broth microdilution method according to Clinical and Laboratory Standards Institute (CLSI) guidelines. Bacterial strains were grown overnight on Luria–Bertani (LB) broth at 37 °C with shaking at 120 rpm. Then, bacteria were suspended in Mueller-Hinton (MH) broth. The bacterial suspensions were further diluted in MH broth to obtain a final inoculum of approximately 1×10^6 CFU mL^{-1}. The $PASP_nDA_m$ compound was dissolved in sterile deionized water to prepare a stock solution of 1 mg mL^{-1}. Two-fold serial dilutions were prepared in deionized water in a 96-well microtiter plate (100 μL per well). Each well was inoculated with another 100 μL of the diluted bacterial suspensions (1×10^6 CFU mL^{-1}). Positive (bacteria suspended in equal volumes of MH broth and sterile deionized water) and negative controls (equal volumes of MH broth and sterile deionized water) were included. Plates were incubated at 37 °C for 24 h, and bacterial growth was assessed by measuring absorbance at 600 nm (OD_{600}). The MIC was defined as the lowest concentration of $PASP_nDA_m$ that completely inhibited visible growth of the test organism. The MICs of the $PASP_nDA_m$ against Methicillin-resistant *Staphylococcus aureus* (MRSA) were evaluated according to the same method.

2.3. *In vitro* cytotoxicity assay

L929 mouse fibroblast cells were seeded in 96-well plates at a density of 1×10^4 cells per well in DMEM supplemented with 10% fetal bovine serum and 1% penicillin–streptomycin. The plates were incubated for 24 h at 37 °C in a humidified incubator containing 5% CO_2 to allow cell attachment. $PASP_nDA_m$ was dissolved in sterile medium at a concentration of 1 mg mL^{-1}. Serial two-fold dilutions were prepared in cell culture medium to the desired final concentrations. After culturing for 24 h, the medium was removed and replaced with 100 μL of the $PASP_nDA_m$ solutions (A_{sample}). Cells treated with medium only served as the non-toxic negative control ($A_{control}$). One hundred microliters of each dilution was added to the wells, with untreated cells serving as the negative control and wells containing only medium serving as the blank control. Each concentration was tested in triplicate. The plates were incubated for an additional 24 h. After 24 h, 10 μL of MTT solution in PBS (5 mg mL^{-1}) was added to each well. The plates were returned to the incubator for 4 h to allow metabolically active cells to form formazan crystals. The MTT solution was then discarded, and the insoluble formazan crystals were dissolved in 150 μL of DMSO per well with gentle shaking for 10 min. The absorbance was measured at 492 nm using a microplate reader. Cell viability was calculated as

$$\text{Cell viability } (\%) = OD_{420}(A_{sample})/OD_{420}(A_{control}) \times 100\%. \quad (1)$$

The polymer concentration that inhibited 50% of cell growth (IC_{50}) was determined by non-linear regression analysis.

2.4. *In vivo S. aureus*-infected mouse wound model

Female Kunming mice (6–8 weeks old, weighing 18–20 g) were purchased from Liaoning Changsheng Biotechnology Ltd (Liaoning, China). All animal procedures were performed in accordance with the Guidelines for Care and Use of Laboratory Animals of Jilin University and approved by the Animal Ethics Committee of Jilin University.

An *in vivo* model of *S. aureus*-infected mouse wounds was established by inducing standardized wounds (d = 10 mm) on the epidermis of mice, followed by inoculation with *S. aureus*. After 24 h of wound infection, mice were treated with a topical solution containing $PASP_{10}DA_6$ on days 3, 5, and 7. In the PBS group (PG), only *S. aureus* infection was applied. In the vancomycin treatment group (VG), 20 μg mL^{-1} vancomycin was used for the treatment. In the low-concentration $PASP_{10}DA_6$ treatment group (LG), 50 μg mL^{-1} $PASP_{10}DA_6$ prepared in sterile water was administered after bacterial infection, while in the high-concentration $PASP_{10}DA_6$ treatment group (HG), 100 μg mL^{-1} $PASP_{10}DA_6$ prepared in sterile water was used for treatment after bacterial infection. The non-infected group (NG) served as a model where wounds were created without bacterial infection. Skin samples were collected from the infected sites 24 h after the initial treatment (days 4) to assess bacterial burden. Samples were then homogenized and plated for bacterial enumeration. Additionally, photographs of the wound site were taken every two days to monitor the progression of infection and wound healing. On day 14, mice were euthanized, and wound skin samples were collected for histological examination. Hematoxylin and eosin (H&E) staining and Masson's trichrome staining were performed to evaluate tissue morphology, inflammation, and wound healing. Furthermore, vital organs, including the heart, liver, spleen, lungs, and kidneys, were harvested and subjected to histological examination using H&E staining to assess potential systemic effects of $PASP_{10}DA_6$ treatment. Blood samples were collected for routine blood analysis to evaluate systemic toxicity after treatment with $PASP_{10}DA_6$.

3. Results and discussion

3.1. Synthesis and characterization of $PASP_nDA_m$

The synthetic pathway of $PASP_nDA_m$ is illustrated in Fig. 1a. The ^1H NMR spectrum confirmed the successful synthesis of β-benzyl L-aspartic acid *N*-carboxyanhydride (BLA-NCA), with a singlet peak at 6.31 ppm assigned to the NH proton of the NCA ring, a methine peak d (–CO–CH–NH–) at approximately 4.59 ppm, and a methylene peak e (–CH–CH_2–CO–) at 3.15–2.77 ppm, consistent with the expected structure (Fig. 1b).[29] Different DPs of $PBLA_n$ were synthesized using the ring-opening polymerization of BLA-NCA, where n denotes the feeding molar ratio of BLA-NCA (monomer) to *n*-hexylamine (initiator). The molecular weight (M_n and M_w) and polydispersity indices ($Đ$) of $PBLA_n$ were determined by gel permeation chromatography (GPC) (Fig. S1). The M_n values of $PBLA_{10}$, $PBLA_{20}$, $PBLA_{30}$, and $PBLA_{40}$ obtained by GPC were 2100, 4100,

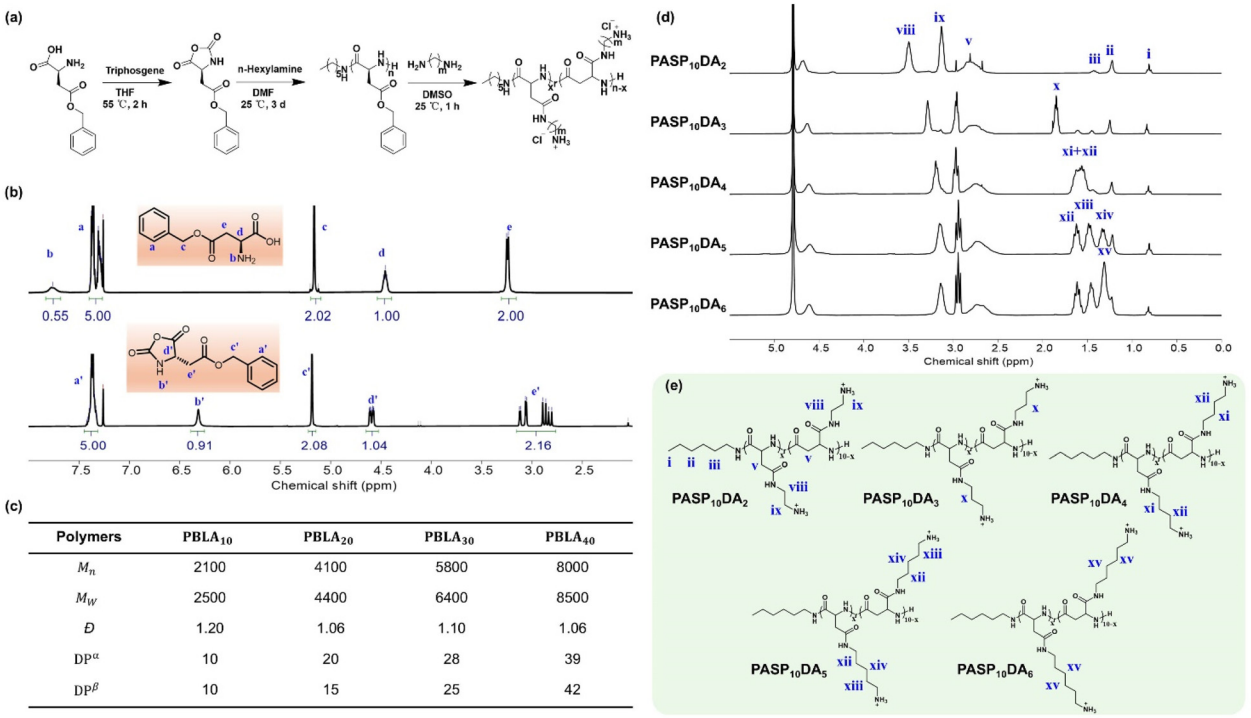

(c)

Polymers	$PBLA_{10}$	$PBLA_{20}$	$PBLA_{30}$	$PBLA_{40}$
M_n	2100	4100	5800	8000
M_W	2500	4400	6400	8500
$Đ$	1.20	1.06	1.10	1.06
DP^{α}	10	20	28	39
DP^{β}	10	15	25	42

Fig. 1 Synthesis of $PASP_nDA_m$. (a) Synthesis scheme for $PASP_nDA_m$ *via* ring-opening and aminolysis reactions. Here, *n* stands for the DP (*n* = 10, 20, 30, and 40), and *m* stands for the number of carbon atoms in the linear diamines (*m* = 2, 3, 4, 5, and 6). (b) ^{1}H NMR spectra of BLA in deuterated chloroform, with a few drops of deuterated trifluoroacetic acid, and BLA-NCA in deuterated chloroform. (c) Molecular weight, DP, and polydispersity of $PBLA_n$ determined by GPC and ^{1}H NMR spectroscopy, where α is calculated from the number-average molecular weight obtained by GPC; β is determined from the ^{1}H NMR spectrum of PBLA. (d) ^{1}H NMR spectra of $PASP_{10}DA_m$ *via* aminolysis (*m* = 2, 3, 4, 5, and 6). (e) Chemical structure of $PASP_{10}DA_m$.

5800, and 8000 g mol^{-1}, respectively, corresponding to DPs of 10, 20, 28, and 39, which closely match the feeding ratios of BLA-NCA to *n*-hexylamine, and these polymers showed low $Đ$ values, ranging from 1.20 to 1.06 (Fig. 1c). The DP of PBLA was also decided from the proton nuclear magnetic resonance (^{1}H NMR) spectrum (Fig. S2–S5) by comparing the integral ratio of the peak area at 7.0–7.2 ppm (the benzene ring) with that at 0.7 ppm (the methyl group of the *n*-hexylamine end group). The DPs of $PBLA_{10}$, $PBLA_{20}$, $PBLA_{30}$, and $PBLA_{40}$ calculated from the ^{1}H NMR spectra were 10, 15, 25, and 42, respectively, which are also close to the feeding ratios of BLA-NCA to *n*-hexylamine.[27,28] $PASP_nDA_m$ polymers were successfully synthesized through the aminolysis of PBLA using linear diamines. The ^{1}H NMR spectrum of $PASP_{10}DA_m$ revealed the disappearance of peaks corresponding to the benzyl ring (7.0–7.2 ppm) and the benzylic methylene (4.9–5.0 ppm). Peaks corresponding to the initiator (*n*-hexylamine, CH_3CH_2–) remained unchanged, while new methylene peaks (1.0–2.0 ppm) from the linear diamines were observed (Fig. 1d and e). The DP of these polyaspartamides showed no significant change. These observations suggested that the linear diamines were successfully grafted onto the polypeptide backbone. $PASP_{10}DA_2$, $PASP_{10}DA_3$, $PASP_{10}DA_4$, $PASP_{10}DA_5$ and $PASP_{10}DA_6$ were successfully synthesized. Similarly, PBLA polymers with other DPs (20, 30 and 40) were successfully aminolyzed using linear diamines of varying side chain lengths (Fig. S6–S20).

3.2. Antibacterial activity and biocompatibility of $PASP_nDA_m$

We conducted a systematic evaluation of the antimicrobial efficacy of these $PASP_nDA_m$ against both Gram-positive (*S. aureus*) and Gram-negative (*E. coli*) bacteria by assessing their ability to inhibit bacterial growth (Fig. S21). All $PASP_nDA_m$ exhibited inhibitory activity against both *S. aureus* and *E. coli*. As displayed in Fig. 2a and Table S1, $PASP_{10}DA_5$ exhibited the weakest inhibitory effect against *S. aureus*, with an MIC of 125 μg mL^{-1}, while $PASP_{40}DA_4$ showed the strongest inhibition, with the lowest MIC of 3.9 μg mL^{-1}. Most $PASP_{40}DA_m$ samples showed lower MIC values compared to $PASP_{10}DA_m$, showing that increasing the DP could contribute to the improved antibacterial effectiveness. Moreover, in most cases, $PASP_nDA_6$ (*n* = 10, 20, 30, and 40) consistently presented lower MIC than polypeptides with other diamine side chains. For example, the MIC of $PASP_{10}DA_6$ against *S. aureus* was 7.8 μg mL^{-1}, which was significantly lower than those of $PASP_{10}DA_m$ (*m* = 2, 3, 4 and 5). Like the inhibitory effect against *S. aureus*, $PASP_nDA_m$ also proved an inhibitory effect against *E. coli*. The MICs of $PASP_{10}DA_2$ and $PASP_{10}DA_5$ were 62.5 μg mL^{-1}, while $PASP_{10}DA_6$ and $PASP_{40}DA_3$ exhibited significantly lower MICs of 7.8 μg mL^{-1} (Fig. 2b and Table S2). Interestingly, $PASP_{10}DA_6$

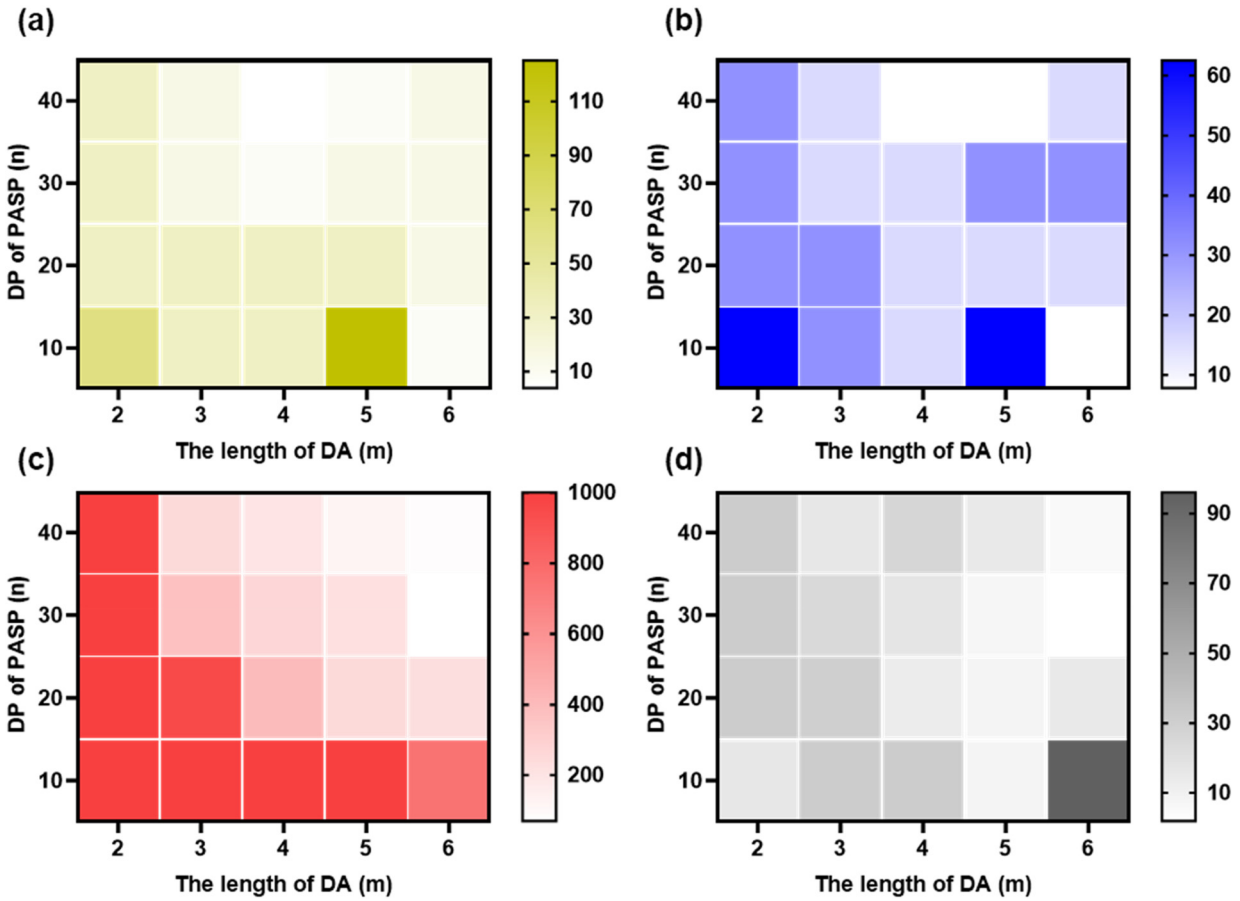

Fig. 2 Antibacterial effect and toxicity of $PASP_nDA_m$. (a) MIC of $PASP_nDA_m$ against *S. aureus* (μg mL^{-1}). (b) MIC of $PASP_nDA_m$ against *E. coli* (μg mL^{-1}). (c) IC_{50} values of $PASP_nDA_m$ against L929 cells (μg mL^{-1}). (d) Selectivity index of $PASP_nDA_m$ (calculated as the ratio of IC_{50} for L929 cells to MIC against *S. aureus*).

maintained its effectiveness in killing *E. coli*, which suggested that $PASP_{10}DA_6$ could effectively kill both Gram-negative and Gram-positive bacteria. Generally, the observed variations in MIC across different $PASP_nDA_m$ suggest that both the DP and side chain length play critical roles in the antimicrobial activity of $PASP_nDA_m$. Higher DP appeared to enhance the interaction of the polymer with bacteria, leading to enhanced membrane disruption activity.[30,31] At DPs of 10 and 20, the antibacterial activity of $PASP_nDA_m$ increased with increasing side chain length. However, at DPs of 30 and 40, antibacterial activity initially increased and then decreased as the side chain length increased. The length of the side chain had a notable influence on the antimicrobial activity of $PASP_{10}DA_m$; as the side-chain carbon number increased from 2 to 6, the MIC of $PASP_{10}DA_m$ decreased from 125 to 7.8 μg mL^{-1}. For side chain containing 2, 3, 4 and 5 carbon atoms, the antibacterial activity of $PASP_nDA_m$ increased with increasing DP. In contrast, for a side chain with 6 carbon atoms, a slightly opposite trend was observed. In addition, we verified the antibacterial properties of the polymers against clinically drug-resistant bacteria. As shown in Table S3, $PASP_nDA_m$ showed certain antibacterial performance against MRSA. Considering the complex environment of infected tissues, we examined whether the antibacterial activity of $PASP_{10}DA_6$ would be affected under variable conditions. After different treatments, the MIC value of $PASP_{10}DA_6$ remained unchanged (Table S4), demonstrating the good stability of the polymer.

Further experiments were conducted to evaluate the cytotoxicity and hemolytic effects of these polypeptides. The cytotoxicity and hemolytic activities of $PASP_nDA_m$ were measured against the mouse fibroblast cell line L929 (Fig. S22) and rabbit red blood cells (Fig. S23), respectively. $PASP_nDA_2$ and $PASP_{10}DA_m$ exhibited good biocompatibility, with IC_{50} values around 1000 μg mL^{-1}; however, most of these had low antimicrobial activity. Notably, $PASP_nDA_6$ showed a trend of increased cytotoxicity with increasing DP. The IC_{50} value was 750 μg mL^{-1} for $PASP_{10}DA_6$, which decreased to 80 μg mL^{-1} for $PASP_{40}DA_6$ (Fig. 2c and Table S5). Based on these observations, the cytotoxicity risk of $PASP_nDA_m$ against L929 cells increases with both the DP and side chain length. Regarding hemolytic activity, most $PASP_nDA_m$ samples showed HC_5 values greater than 2000 μg mL^{-1}, showing that these polymers were well-tolerated by red blood cells (Table S6). This suggests a low possibility of causing hemolysis by $PASP_nDA_m$ at

a concentration around their MIC values. Based on the antibacterial and cytotoxicity assays, the selectivity index (SI) was then calculated as the ratio of IC_{50} for L929 cells to the MIC against *S. aureus* to evaluate the balance between antimicrobial activity and cytotoxicity (Table S7). Due to its low MIC values against bacteria and high IC_{50} values for L929 cells, $PASP_{10}DA_6$ exhibited the highest SI of 96 among all tested $PASP_nDA_m$ (Fig. 2d), showing that $PASP_{10}DA_6$ could be an effective and safe therapeutic agent.

3.3. Bactericidal mechanisms of $PASP_{10}DA_6$

To evaluate the antibacterial mechanism of $PASP_{10}DA_6$, scanning electron microscopy (SEM) was used to reveal surface alterations in *S. aureus* and *E. coli* following treatment with the $PASP_{10}DA_6$. After treatment with $PASP_{10}DA_6$, obvious morphological changes were observed on the surfaces of both *S. aureus* and *E. coli*, characterized by surface depressions and blurred boundaries on the bacteria (Fig. 3a). By contrast, negligible alterations were observed in the morphology of bacteria treated with norfloxacin and PBS. Norfloxacin exerts its bactericidal effect by inhibiting bacterial DNA gyrase and topoisomerase IV, essential enzymes involved in bacterial DNA replication and transcription.[32] This mechanism effectively halts bacterial proliferation without causing significant changes to bacterial surface morphology. Next, a live/dead assay was conducted to further investigate bacterial membrane damage after treatment with $PASP_{10}DA_6$. The simultaneous use of SYTO 9 and PI dyes allowed differentiation between live and damaged bacteria, *i.e.*, viable bacteria with intact membranes exhibit strong green fluorescence and minimal PI uptake, while bacteria with damaged membranes show increased red fluorescence from PI and potentially reduced SYTO 9 signals.[33] Following a 3-hour exposure period, $PASP_{10}DA_6$-treated samples displayed a higher proportion of red-stained bacteria under fluorescence microscopy compared to norfloxacin-treated samples. By contrast, PBS and norfloxacin treatment groups showed no significant red fluorescence, suggesting that these treatments do not disrupt bacterial membranes. Therefore, the presence of red fluorescence in the $PASP_{10}DA_6$-treated group confirmed its ability to induce membrane damage (Fig. 3b and S24).

To gain further insights into the antibacterial mechanism of $PASP_{10}DA_6$, the interaction between $PASP_{10}DA_6$ and the bacterial membrane was investigated. The relationship between the antimicrobial efficacy of polypeptides and their secondary structures is a crucial aspect of understanding their mode of

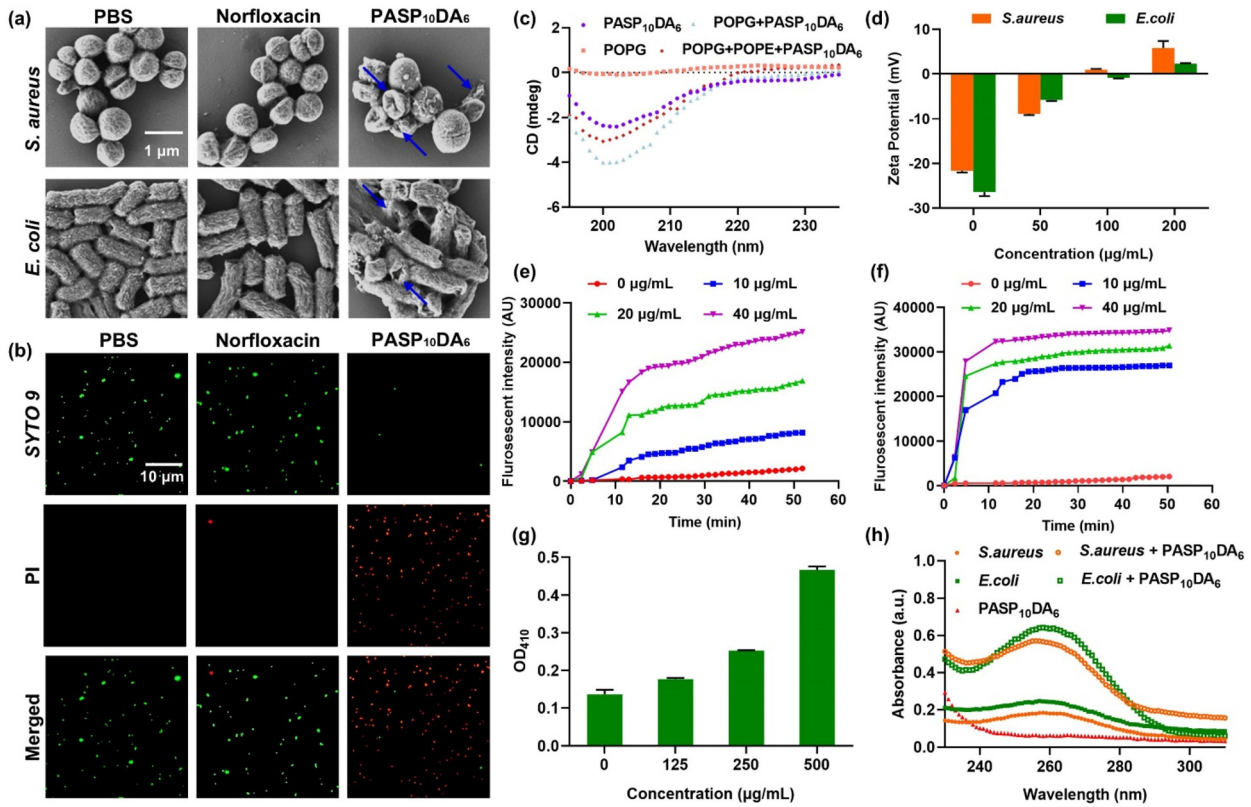

Fig. 3 Bactericidal mechanism of $PASP_{10}DA_6$ against *S. aureus* and *E. coli*. (a) SEM images of *S. aureus* and *E. coli* after treatment with 1 × MIC of norfloxacin (0.04 μg mL^{-1}) and $PASP_{10}DA_6$. (b) Fluorescence images of *S. aureus* post-treatment with 1 × MIC norfloxacin (0.04 μg mL^{-1}) and $PASP_{10}DA_6$. (c) CD spectra of $PASP_{10}DA_6$ before and after interaction with POPG or POPG + POPE. (d) Surface potential alterations in *S. aureus* and *E. coli*. exposed to $PASP_{10}DA_6$. (e) Membrane depolarization effects of $PASP_{10}DA_6$ on *S. aureus*. (f) Membrane depolarization effects of $PASP_{10}DA_6$ on *E. coli*. (g) Permeability of the *E. coli* membrane in response to $PASP_{10}DA_6$ exposure. (h) Leakage of nucleic acids from *S. aureus* and *E. coli* treated with $PASP_{10}DA_6$.

action.[34] Our observations revealed that $PASP_{10}DA_6$ remained in a random coil conformation in both pure and POPG-containing aqueous solution (Fig. 3c). $PASP_{10}DA_6$ did not undergo secondary structural changes when transitioning from pure aqueous solution to membrane-simulating environments (POPG-containing solutions), suggesting that its antibacterial activity does not rely on a transition of secondary structure. The absence of a secondary structure transition upon membrane interaction may contribute to the low cytotoxicity of $PASP_{10}DA_6$. This was because keeping a random coil conformation could reduce its tendency to insert into mammalian cell membranes, thereby minimizing membrane disruption and cytotoxic effects.[35] Adsorption of cationic polypeptides onto the negatively charged surfaces of bacteria can result in alterations in the bacterial ζ-potential. As shown in Fig. 3d, when the concentration of $PASP_{10}DA_6$ was 50 μg mL^{-1}, the surface potential of the bacteria increased by 10 mV. The shift in the bacterial ζ-potential suggests that the cationic $PASP_{10}DA_6$ successfully binds to the bacterial membrane through electrostatic interactions. The action of $PASP_{10}DA_6$ on the bacterial membrane was further investigated through membrane depolarization experiments. As displayed in Fig. 3e and f, $PASP_{10}DA_6$ demonstrated its potential in disrupting bacterial homeostasis through significant membrane depolarization in both *S. aureus* and *E. coli*. The degree of membrane depolarization increased with increasing concentrations of $PASP_{10}DA_6$. This result provided evidence of the polypeptide's ability to destabilize bacterial membranes, leading to impaired bacterial function and contributing to its antimicrobial effect.[36]

The *ortho*-nitrophenyl-β-galactoside (ONPG) cleavage method is particularly useful in the study of the effects of polypeptides on the integrity of bacterial membranes. ONPG cannot traverse the bacterial membrane to be cleaved by cytoplasmic β-galactosidase into the yellow compound *o*-nitrophenol (ONP) unless permeabilization of the bacterial membrane is increased.[37] Enhanced permeability changes were observed in *E. coli* and *S. aureus* exposed to $PASP_{10}DA_6$, as indi-

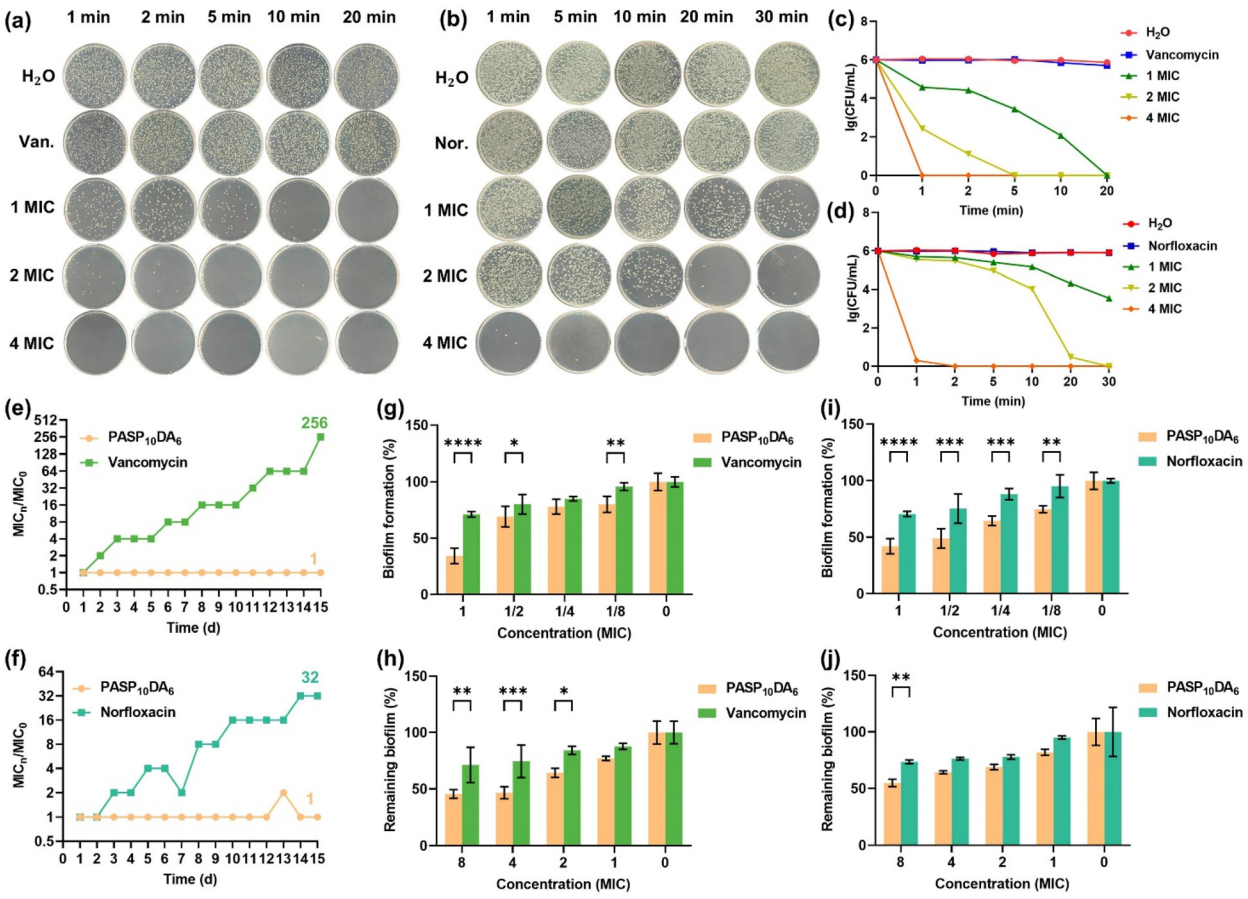

Fig. 4 Antimicrobial activity and resistance induction by $PASP_{10}DA_6$. (a) Time-dependent plating results for *S. aureus* treated with $PASP_{10}DA_6$; "van." means vancomycin (2 μg mL^{-1}). (b) Time-dependent plating results for *E. coli* treated with $PASP_{10}DA_6$; "nor." means norfloxacin (0.04 μg mL^{-1}). (c) Survival of *S. aureus* at different time points following incubation with antimicrobial agents, based on data given in (a). (d) Survival of *E. coli* at different time points following incubation with antimicrobial agents, based on data given in (b). (e) Resistance induction in *S. aureus* by vancomycin and $PASP_{10}DA_6$. (f) Resistance induction in *E. coli* by norfloxacin and $PASP_{10}DA_6$. (g) Inhibition of *S. aureus* biofilm formation by $PASP_{10}DA_6$, using vancomycin (MIC = 2 μg mL^{-1}) as a control. (h) Biofilm dispersion in mature *S. aureus* cultures. (i) Inhibition of *E. coli* biofilm formation by $PASP_{10}DA_6$, with norfloxacin (MIC = 0.04 μg mL^{-1}) as a control. (j) Dispersion of mature *E. coli* biofilms. *$p < 0.05$, **$p < 0.01$, and ***$p < 0.001$.

cated by increased ONPG cleavage (Fig. 3g and S25). The observed increase in membrane permeability further confirms the results of the bacterial membrane depolarization after treatment with polypeptides.[38–40] Furthermore, nucleic acid leakage from bacteria after the treatment with $PASP_{10}DA_6$ was investigated by UV-Vis absorption spectroscopy (Fig. 3h). Peaks at 260 nm were clearly observed after treatment with $PASP_{10}DA_6$, indicating a large amount of nucleic acid leakage.[41,42] Taken together, all the abovementioned results indicate that the antimicrobial mechanism of $PASP_{10}DA_6$ involves the binding of $PASP_{10}DA_6$ to bacterial membranes *via* electrostatic interactions, triggering membrane depolarization and disruption.

3.4. Killing kinetics, resistance development, and biofilm disruption of $PASP_{10}DA_6$

It has been reported that AMPs exhibit more rapid bactericidal kinetics than antibiotics.[43] Accordingly, we investigated the bactericidal rate of $PASP_{10}DA_6$. Antimicrobial kinetics analysis revealed the rapid bactericidal action of $PASP_{10}DA_6$ (Fig. 4a and b). Specifically, $PASP_{10}DA_6$ eliminated 100% of *S. aureus* within 20 min at 1 × MIC, while 2 × MIC was required to achieve similar effects against *E. coli*. The killing rate of Gram-negative bacteria was slightly lower compared to Gram-positive bacteria, possibly due to the presence of the outer membrane in Gram-negative bacteria.[44] At 4 × MIC, $PASP_{10}DA_6$ effectively eradicated all bacteria within approximately 1 min. By contrast, vancomycin and norfloxacin did not show significant bactericidal activity within 20 min, similar to the control group (Fig. 4c and d). These results highlight that the bactericidal efficacy of $PASP_{10}DA_6$ is both time- and concentration-dependent. Moreover, the membrane-disrupting bactericidal mechanism of $PASP_{10}DA_6$ leads to rapid bacterial death, which differs from the mechanisms of vancomycin and norfloxacin.

Bacterial resistance to antibiotics is a significant global health threat.[45,46] This resistance not only complicates treatment strategies but also increases healthcare costs. Unlike traditional antibiotics, most AMPs act on bacterial membranes, a mechanism that reduces the likelihood of resistance development.[47–49] As expected, over a 15-day period, $PASP_{10}DA_6$ did not induce bacterial resistance in both *S. aureus* and *E. coli*, while the MIC values of vancomycin and norfloxacin increased by 256-fold and 32-fold, respectively (Fig. 4e and f). The absence of resistance development in bac-

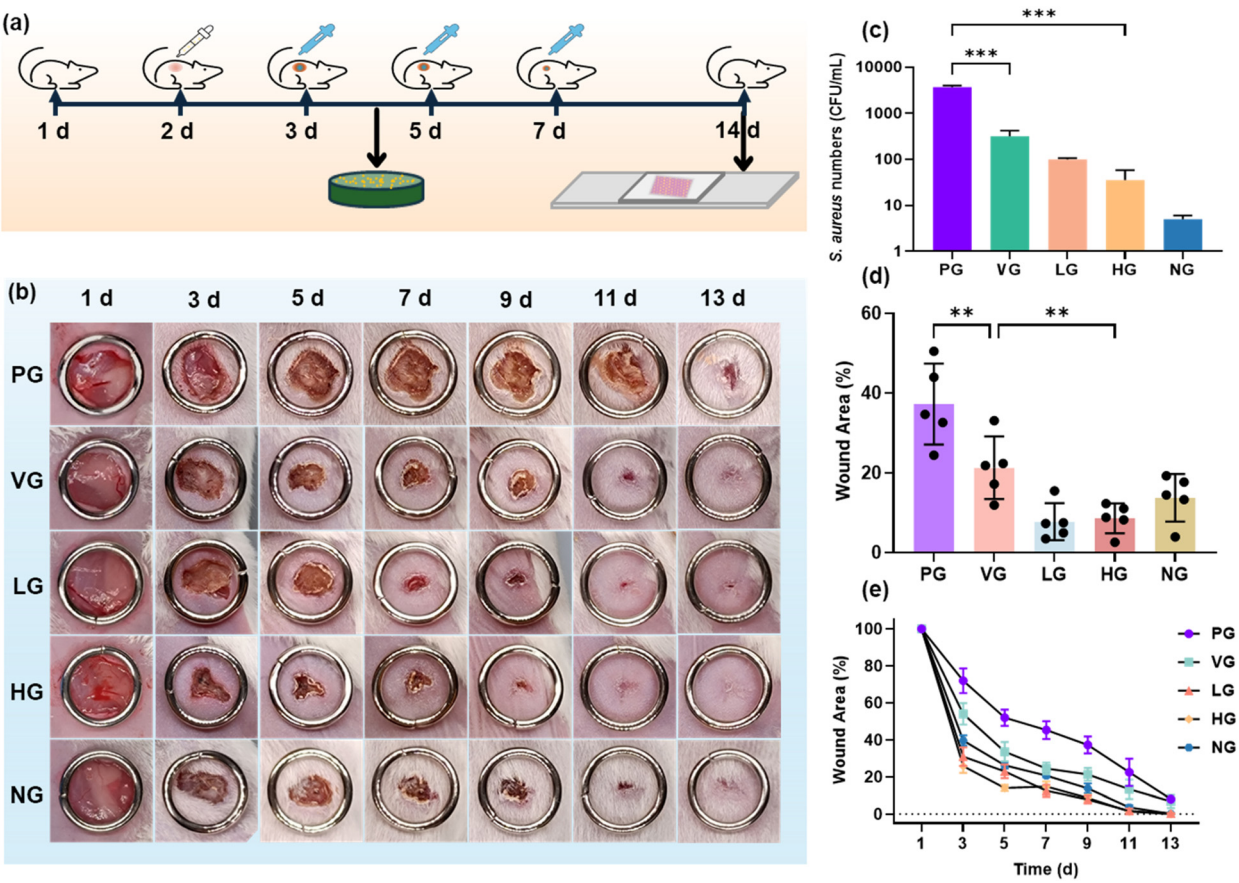

Fig. 5 Application of $PASP_{10}DA_6$ in the treatment of murine skin infection. (a) Timeline of $PASP_{10}DA_6$ administration and sample collection points. (b) Representative images of infected skin wounds after treatment (ring diameter: 10 mm). (c) Bacterial count results from the tissue coating plates after fragmentation of infected tissues on day 4. (d) Bar graph comparing wound area percentages across different groups on the seventh day. (e) Quantitative analysis of lesion size over the treatment period. *p < 0.05, **p < 0.01, and ***p < 0.001. Error bars indicate standard deviation (n = 5).

teria treated with $PASP_{10}DA_6$ emphasizes its potential as a sustainable antimicrobial strategy.

Biofilms, formed by microbial communities, pose significant hazards, as they provide protection for pathogens, promote antibiotic resistance, and cause surface contamination to increase the risk of chronic infections.[50] Preventing and controlling biofilm formation are crucial for keeping environmental hygiene, reducing healthcare-associated infections, and safeguarding human health.[51–53] Therefore, we evaluated the inhibition effect of $PASP_{10}DA_6$ on the formation of biofilm. As shown in Fig. 4g, $PASP_{10}DA_6$ markedly inhibited the formation of *S. aureus* biofilms compared to vancomycin, reducing biofilm formation rate by 65% and 31% for $PASP_{10}DA_6$ and vancomycin, respectively. For mature biofilms, $PASP_{10}DA_6$ at 8-fold MIC dispersed approximately 55% of the biofilm mass, significantly outperforming vancomycin, which only achieved 24% dispersion (Fig. 4h). For *E. coli*, $PASP_{10}DA_6$ showed a 58% reduction in biofilm formation at 1-fold MIC, surpassing the 30% reduction by norfloxacin at 1-fold MIC (Fig. 4i). $PASP_{10}DA_6$ also proved a strong dispersion effect on mature *E. coli* biofilms, disrupting up to 46% at 8-fold MIC compared to 27% by norfloxacin (Fig. 4j). The inhibitory and eradication effects of $PASP_{10}DA_6$ on biofilms were superior to those of antibiotics at the same MIC.

3.5. *In vivo* antibacterial efficacy

Inspired by the high antibacterial activity and good biocompatibility of $PASP_{10}DA_6$, we evaluated the therapeutic efficacy of $PASP_{10}DA_6$ against *S. aureus*-infected epidermal wounds. Bacterial infections were induced in epidermal wounds, fol-

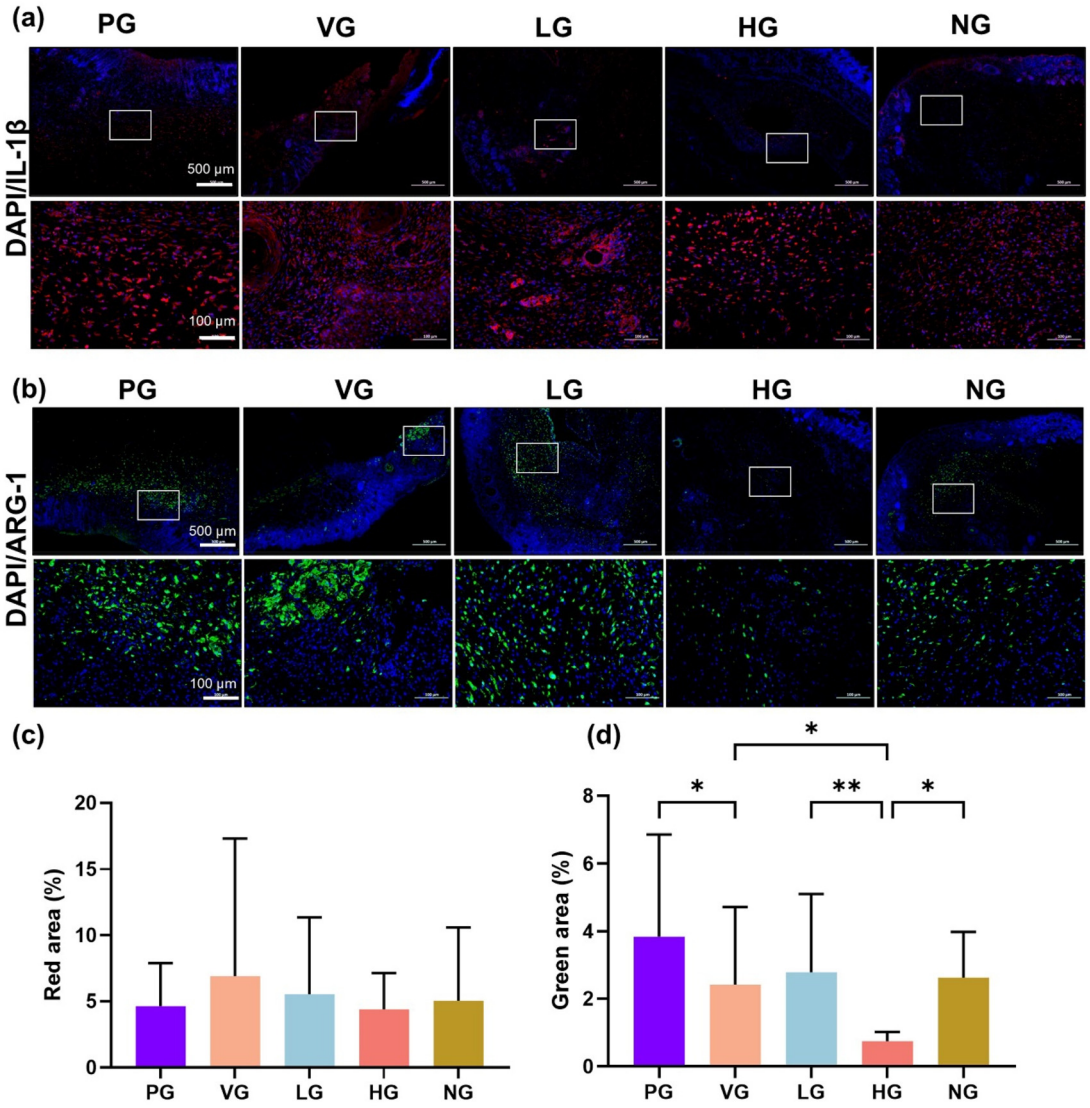

Fig. 6 Immunofluorescence analysis of mouse wound sections. (a) Immunofluorescence staining for IL-1β (red) and cell nuclei with DAPI (blue). (b) Immunofluorescence staining for ARG-1 (green) and cell nuclei with DAPI (blue). (c) Quantification of relative areas of red fluorescence (IL-1β). (d) Quantification of relative areas of green fluorescence (ARG-1). Statistical significance is denoted as $*p < 0.05$, $**p < 0.01$, and $***p < 0.001$.

lowed by treatment with $PASP_{10}DA_6$ and vancomycin. The progression of infection and wound healing was monitored to assess the effectiveness of $PASP_{10}DA_6$ in reducing bacterial burden and promoting recovery under physiological conditions. The mice were divided into five groups: the PBS group (PG, infected but non-treated), vancomycin treatment group (VG, 20 μg mL^{-1}), low-concentration $PASP_{10}DA_6$ treatment group (LG, 50 μg mL^{-1}), high-concentration $PASP_{10}DA_6$ treatment group (HG, 100 μg mL^{-1}), and the non-infected group (NG). The timeline and sampling points were carefully planned to capture both immediate and extended impacts of the treatments (Fig. 5a). Representative images illustrate the progression of infected skin lesions during treatment (Fig. 5b), with the diameter of the infected area visibly decreasing in the $PASP_{10}DA_6$-treated groups. On the fourth day, $PASP_{10}DA_6$ was able to eliminate more than 99% of the bacteria at the wound site, while vancomycin treatment achieved a reduction of only 90% (Fig. 5c). Due to its significant reduction of bacterial burden at the wound site, the $PASP_{10}DA_6$-treated group showed a notably smaller wound area on day seven compared to the PG and the VG (Fig. 5d). Throughout the wound healing process, the VG and $PASP_{10}DA_6$-treated groups showed comparable effects in reducing wound area (Fig. 5e). These findings indicate that $PASP_{10}DA_6$ could effectively kill bacteria and then accelerate the wound healing process.

IL-1β (Interleukin-1β), a marker of pro-inflammatory M1 macrophages, indicated an active inflammatory response associated with bacterial infection in the mouse epidermal wound model. Conversely, ARG-1 (Arginase-1), a marker of anti-inflammatory M2 macrophages, suggested a transition toward tissue repair and resolution of infection, reflecting controlled inflammation and progression toward wound healing. Fluorescence staining with DAPI/IL-1β, as well as DAPI/ARG-1, was performed to analyze the healing of the mouse wound (Fig. 6a and b). In the later stages of wound healing, red fluorescence was predominantly localized in the wound area, and there were no significant differences in IL-1β fluorescence among all groups, which might reflect that inflammation in the wound had reached a steady state by the end of treatment (Fig. 6c). However, differences were observed in ARG-1 fluorescence levels across the groups. The HG exhibited the lowest green fluorescence intensity for ARG-1, lower than that of the NG group. Conversely, the PG demonstrated the highest fluorescence intensity, while the VG and the LG showed no significant differences from each other (Fig. 6d). Low ARG-1 expression in the HG indicated that, by the end of the treatment period, wounds in the HG had restored near-normal tissue structure, potentially surpassing the non-infected NG. By contrast, high ARG-1 expression in the PG suggested ongoing rapid tissue repair. These results aligned with H&E staining observations. These results indicate that $PASP_{10}DA_6$ could promote wound healing and tissue repair.

Following the animal experiments, physiological toxicity assessments were conducted to ensure the antimicrobial efficacy without causing significant harm to normal tissues. Histological examination of heart, liver, spleen, lung, and kidney tissues revealed no significant changes (Fig. S26), indicating minimal biotoxicity of $PASP_{10}DA_6$. Hematological analysis further supported the biocompatibility of $PASP_{10}DA_6$. Hematological results showed no significant changes in white blood cells (WBC), lymphocytes (LYM), neutrophils (NEU), platelets (PLT), red blood cells (RBC), or hemoglobin (HGB) levels (Fig. S27), indicating that $PASP_{10}DA_6$ did not cause immune activation, inflammation, or hematological abnormalities. These results indicate that $PASP_{10}DA_6$ is a safe and effective antibacterial poly(amino acid) suitable for treating bacterial infections.

4. Conclusion

In summary, this study systematically investigated the impact of side chain lengths and DP on the antibacterial properties of polyaspartamides. *In vitro* antibacterial experiments showed that antimicrobial activity increased with increasing length of side chains and DP. However, when the DP of $PASP_nDA_m$ exceeded 20, further increases in DP did not improve antimicrobial efficacy of $PASP_nDA_m$ but instead led to increased hemolytic and cytotoxic effects. Among all the tested $PASP_nDA_m$, $PASP_{10}DA_6$ exhibited a relatively low MIC and the highest selectivity against both *S. aureus* and *E. coli*. The antimicrobial mechanism of $PASP_{10}DA_6$ involved adsorption onto negatively charged bacterial surfaces *via* electrostatic interactions and disruption of membrane integrity. Unlike traditional antibiotics, $PASP_{10}DA_6$ did not induce bacterial resistance and was more effective in the inhibition of biofilm formation and dispersion of mature biofilms. *In vivo* antibacterial studies demonstrated that $PASP_{10}DA_6$ not only effectively eradicates bacterial pathogens but also promoted wound healing. These findings underscore the potential of $PASP_{10}DA_6$ as a valuable antimicrobial agent with promising applications for treating infections that require biofilm prevention and resistance management.

Author contributions

Wenlong Zhang: writing—original draft, investigation, formal analysis, and methodology; Guowenlie Gao: formal analysis and methodology; Yuqian Ji: formal analysis and methodology; Mingming Zhao: formal analysis; Pengqi Wan: writing—review and editing, supervision, and funding acquisition; Chunsheng Xiao: writing—review and editing, conceptualization, supervision, investigation, formal analysis, resources, and funding acquisition; Xuesi Chen: writing—review and editing, conceptualization, supervision, investigation, formal analysis, and resources. All the authors approved the final version of the manuscript.

Conflicts of interest

There are no conflicts to declare.

Data availability

The data supporting this article have been included as part of the SI.

The Supplementary Information provides additional experimental section, NMR spectra of intermediates and polymers, and supporting figures that complement the main findings of the study. See DOI: **https://doi.org/10.1039/d5bm00994d**.

Acknowledgements

The work was financially supported by the National Natural Science Foundation of China (52222307, U21A2089) and the Youth Growth Technology Project of the Jilin Provincial Department of Science and Technology (20230508153RC).

References

1 S. Dhingra, N. A. A. Rahman, E. Peile, M. Rahman, M. Sartelli, M. A. Hassali, T. Islam, S. Islam and M. Haque, *Front. Public Health*, 2020, **8**, 535668.
2 D. Jia, Y. Zou, J. Cheng, Y. Zhang, H. Zhang, K. Lu, H. Chen, Y. Zhang and Q. Yu, *J. Mater. Sci. Technol.*, 2025, **205**, 98–108.
3 J. M. A. Blair, M. A. Webber, A. J. Baylay, D. O. Ogbolu and L. J. V. Piddock, Molecular Mechanisms of Antibiotic Resistance, *Nat. Rev. Microbiol.*, 2015, **13**(1), 42–51.
4 E. M. Darby, E. Trampari, P. Siasat, M. S. Gaya, I. Alav, M. A. Webber and J. M. A. Blair, Molecular Mechanisms of Antibiotic Resistance Revisited, *Nat. Rev. Microbiol.*, 2023, **21**(5), 280–295.
5 D. L. Paterson and P. N. A. Harris, *Lancet Infect. Dis.*, 2016, **16**, 132–133.
6 S. McCallin, T. M. Kessler and L. Leitner, *Clin. Microbiol. Infect.*, 2023, **29**, 1267–1271.
7 Y. Wu, D. Jia, K. Lu, H. Zhang, C. Liu, Y. Lin, J. Cheng, Y. Zou, H. Xu, H. Chen, Y. Zhang and Q. Yu, *J. Mater. Sci. Technol.*, 2023, **160**, 76–85.
8 B. H. Gan, J. Gaynord, S. M. Rowe, T. Deingruber and D. R. Spring, The Multifaceted Nature of Antimicrobial Peptides: Current Synthetic Chemistry Approaches and Future Directions, *Chem. Soc. Rev.*, 2021, **50**(13), 7820–7880.
9 C. Wang, T. Hong, P. Cui, J. Wang and J. Xia, Antimicrobial Peptides towards Clinical Application: Delivery and Formulation, *Adv. Drug Delivery Rev.*, 2021, **175**, 113818.
10 W. Shen, P. He, C. Xiao and X. Chen, From Antimicrobial Peptides to Antimicrobial Poly(A-amino Acid)s, *Adv. Healthcare Mater.*, 2018, **7**(20), 1800354.
11 P. Salas-Ambrosio, A. Tronnet, P. Verhaeghe and C. Bonduelle, Synthetic Polypeptide Polymers as Simplified Analogues of Antimicrobial Peptides, *Biomacromolecules*, 2021, **22**(1), 57–75.
12 P. Teng, H. Shao, B. Huang, J. Xie, S. Cui, K. Wang and J. Cai, Small Molecular Mimetics of Antimicrobial Peptides as a Promising Therapy To Combat Bacterial Resistance, *J. Med. Chem.*, 2023, **66**(4), 2211–2234.
13 W. Li, X. Xiao, Y. Qi, X. Lin, H. Hu, M. Shi, M. Zhou, W. Jiang, L. Liu, K. Chen, K. Wang, R. Liu and M. Zhou, Host-Defense-Peptide-Mimicking β-Peptide Polymer Acting as a Dual-Modal Antibacterial Agent by Interfering Quorum Sensing and Killing Individual Bacteria Simultaneously, *Research*, 2023, **6**, 0051.
14 M. Zheng, X. Wu, C. Lu, W. Zhang, S. Tang, Y. Luo and D. Liu, Polypept(o)Ide-Based Bactericides: Weapons against Antibioticresistant Bacterial Infections, *Mater. Today Chem.*, 2023, **27**, 101270.
15 P. Wan, W. Guo, Y. Duan, M. Deng and C. Xiao, Photosensitizer–Polypeptide Conjugate with Synergistic Antibacterial Efficacy, *Macromol. Biosci.*, 2022, **22**(7), 2200105.
16 Y. Wu, K. Chen, J. Wang, M. Chen, Y. Chen, Y. She, Z. Yan and R. Liu, Host Defense Peptide Mimicking Antimicrobial Amino Acid Polymers and beyond: Design, Synthesis and Biomedical Applications, *Prog. Polym. Sci.*, 2023, **141**, 101679.
17 S. M. Thombre and B. D. Sarwade, Synthesis and Biodegradability of Polyaspartic Acid: A Critical Review, *J. Macromol. Sci., Part A: Pure Appl. Chem.*, 2005, **42**(9), 1299–1315.
18 H. Adelnia, H. D. N. Tran, P. J. Little, I. Blakey and H. T. Ta, Poly(Aspartic Acid) in Biomedical Applications: From Polymerization, Modification, Properties, Degradation, and Biocompatibility to Applications, *ACS Biomater. Sci. Eng.*, 2021, **7**(6), 2083–2105.
19 H. N. Kovacs, J. Kovacs, M. A. Pisano and B. A. Shidlovsky, Synthesis and Inhibitory Activity of Polyaspartic Acid Derivatives, *J. Med. Chem.*, 1967, **10**(5), 904–908.
20 M. A. Pisano, B. A. Shidlovsky, H. Kovacs and J. Kovacs, Antimicrobial Activity of a Polyaspartic Acid Derivative., *Antimicrob. Agents Chemother.*, 1966, **6**, 457–461.
21 S. Pepeljnjak, B. Zorc and I. Butula, Antimicrobial Activity of Some Hydroxamic Acids, *Acta Pharm.*, 2005, **55**(4), 401–408.
22 A. Sharma, A. A. Pohane, S. Bansal, A. Bajaj, V. Jain and A. Srivastava, Cell Penetrating Synthetic Antimicrobial Peptides (SAMPs) Exhibiting Potent and Selective Killing of Mycobacterium by Targeting Its DNA, *Chem. – Eur. J.*, 2015, **21**(9), 3540–3545.
23 P. S. Yavvari, S. Gupta, D. Arora, V. K. Nandicoori, A. Srivastava and A. Bajaj, Clathrin-Independent Killing of Intracellular Mycobacteria and Biofilm Disruptions Using Synthetic Antimicrobial Polymers, *Biomacromolecules*, 2017, **18**(7), 2024–2033.
24 N. Mauro, D. Schillaci, P. Varvarà, M. G. Cusimano, D. M. Geraci, M. Giuffrè, G. Cavallaro, C. M. Maida and G. Giammona, Branched High Molecular Weight Glycopolypeptide With Broad-Spectrum Antimicrobial Activity for the Treatment of Biofilm Related Infections, *ACS Appl. Mater. Interfaces*, 2018, **10**(1), 318–331.

25 J. Velazco-de-la-Garza, L. Avérous, G. D. J. Sosa-Santillán, E. Pollet, A. Zugasti-Cruz, C. A. Sierra-Rivera, N. V. Pérez-Aguilar and E. Oyervides-Muñoz, Biological Properties of Novel Polysuccinimide Derivatives Synthesized via Quaternary Ammonium Grafting, *Eur. Polym. J.*, 2020, **131**, 109705.

26 A. Torres-Rodriguez, L. Avérous, E. Pollet, G. De Jesús Sosa-Santillán, A. Zugasti-Cruz, C. A. Sierra-Rivera, N. V. Pérez-Aguilar, M. A. Garcia-Lobato and E. Oyervides-Muñoz, Antimicrobial and Anticancer Potential of Novel Polyaspartate Derivatives Synthesized via Quaternary Ammonium Grafting, *J. Appl. Polym. Sci.*, 2022, **139**(38), e52907.

27 S. Yan, S. Chen, X. Gou, J. Yang, J. An, X. Jin, Y. Yang, L. Chen and H. Gao, Biodegradable Supramolecular Materials Based on Cationic Polyaspartamides and Pillar[5] Arene for Targeting Gram–Positive Bacteria and Mitigating Antimicrobial Resistance, *Adv. Funct. Mater.*, 2019, **29**(38), 1904683.

28 M. Nakanishi, J.-S. Park, W.-D. Jang, M. Oba and K. Kataoka, Study of the Quantitative Aminolysis Reaction of Poly(β-Benzyl l-Aspartate) (PBLA) as a Platform Polymer for Functionality Materials, *React. Funct. Polym.*, 2007, **67**(11), 1361–1372.

29 D. Gao, M. Xu, Z. Cao, J. Gao, Y. Chen, Y. Li, Z. Yang, X. Xie, Q. Jiang, W. Wang and J. Liu, Ultrasound-Triggered Phase-Transition Cationic Nanodroplets for Enhanced Gene Delivery, *ACS Appl. Mater. Interfaces*, 2015, 7(24), 13524–13537.

30 B. Deslouches, S. M. Phadke, V. Lazarevic, M. Cascio, K. Islam, R. C. Montelaro and T. A. Mietzner, De Novo Generation of Cationic Antimicrobial Peptides: Influence of Length and Tryptophan Substitution on Antimicrobial Activity, *Antimicrob. Agents Chemother.*, 2005, **49**(1), 316–322.

31 P. Wan, Y. Wang, W. Guo, Z. Song, S. Zhang, H. Wu, W. Yan, M. Deng and C. Xiao, Low-Molecular-Weight Polylysines with Excellent Antibacterial Properties and Low Hemolysis, *ACS Biomater. Sci. Eng.*, 2022, **8**(2), 903–911.

32 K. Drlica and X. Zhao, DNA Gyrase, Topoisomerase IV, and the 4-Quinolones, *Microbiol. Mol. Biol. Rev.*, 1997, **61**(3), 377–392.

33 M. Rosenberg, N. F. Azevedo and A. Ivask, Propidium Iodide Staining Underestimates Viability of Adherent Bacterial Cells, *Sci. Rep.*, 2019, **9**(1), 6483.

34 L. T. Nguyen, E. F. Haney and H. J. Vogel, The Expanding Scope of Antimicrobial Peptide Structures and Their Modes of Action, *Trends Biotechnol.*, 2011, **29**(9), 464–472.

35 H. Zhang, Q. Chen, J. Xie, Z. Cong, C. Cao, W. Zhang, D. Zhang, S. Chen, J. Gu, S. Deng, Z. Qiao, X. Zhang, M. Li, Z. Lu and R. Liu, Switching from Membrane Disrupting to Membrane Crossing, an Effective Strategy in Designing Antibacterial Polypeptide, *Sci. Adv.*, 2023, **9**(4), eabn0771.

36 Z. Si, J. Li, L. Ruan, S. Reghu, Y. J. Ooi, P. Li, Y. Zhu, P. T. Hammond, C. S. Verma, G. C. Bazan, K. Pethe and M. B. Chan-Park, Designer Co-Beta-Peptide Copolymer Selectively Targets Resistant and Biofilm Gram-negative Bacteria, *Biomaterials*, 2023, **294**, 122004.

37 R. I. Lehrer, A. Barton and T. Ganz, Concurrent Assessment of Inner and Outer Membrane Permeabilization and Bacteriolysis in E. Coli by Multiple-Wavelength Spectrophotometry, *J. Immunol. Methods*, 1988, **108**(1–2), 153–158.

38 L. Lin, J. Chi, Y. Yan, R. Luo, X. Feng, Y. Zheng, D. Xian, X. Li, G. Quan, D. Liu, C. Wu, C. Lu and X. Pan, Membrane-Disruptive Peptides/Peptidomimetics-Based Therapeutics: Promising Systems to Combat Bacteria and Cancer in the Drug-Resistant Era, *Acta Pharm. Sin. B*, 2021, **11**(9), 2609–2644.

39 T. G. Johnson and M. J. Langton, Molecular Machines For The Control Of Transmembrane Transport, *J. Am. Chem. Soc.*, 2023, **145**(50), 27167–27184.

40 J.-J. Wu, F. Wang, P.-Q. Wan, L. Pan, C.-S. Xiao, Z. Ma and Y.-S. Li, Synthesis, Characterization of Polyethylene Ionomers and Their Antibacterial Properties, *Chin. J. Polym. Sci.*, 2024, **42**(8), 1077–1084.

41 T. Hua, T. Zhang, Y. Tang, S. Wang, G. Gao, C. Xiao, P. Wan and H. Wu, Poly-(L-homoarginine) for the non-invasive treatment of endophthalmitis, *Mater. Today Bio*, 2025, **33**, 101931.

42 A. O. Nwokeoji, P. M. Kilby, D. E. Portwood and M. J. Dickman, Accurate Quantification of Nucleic Acids Using Hypochromicity Measurements in Conjunction with UV Spectrophotometry, *Anal. Chem.*, 2017, **89**(24), 13567–13574.

43 Q.-Y. Zhang, Z.-B. Yan, Y.-M. Meng, X.-Y. Hong, G. Shao, J.-J. Ma, X.-R. Cheng, J. Liu, J. Kang and C.-Y. Fu, Antimicrobial Peptides: Mechanism of Action, Activity and Clinical Potential, *Mil. Med. Res.*, 2021, **8**(1), 48.

44 H. Nikaido, Molecular Basis of Bacterial Outer Membrane Permeability Revisited, *Microbiol. Mol. Biol. Rev.*, 2003, **67**(4), 593–656.

45 T. R. Walsh, A. C. Gales, R. Laxminarayan and P. C. Dodd, Antimicrobial Resistance: Addressing a Global Threat to Humanity, *PLoS Med.*, 2023, **20**(7), e1004264.

46 W. P. J. Smith, B. R. Wucher, C. D. Nadell and K. R. Foster, Bacterial Defences: Mechanisms, Evolution and Antimicrobial Resistance, *Nat. Rev. Microbiol.*, 2023, **21**(8), 519–534.

47 W. Shang, Q. Sun, C. Zhang, H. Liu, Y. Yang, Y. Liu, W. Gao, W. Shen and D. Yin, Drug in Therapeutic Polymer: Sinomenine-Loaded Oxidation-Responsive Polymeric Nanoparticles for Rheumatoid Arthritis Treatment, *ACS Appl. Mater. Interfaces*, 2023, **15**(40), 47552–47565.

48 W. Shen, Y. Zhang, P. Wan, L. An, P. Zhang, C. Xiao and X. Chen, Antineoplastic Drug–Free Anticancer Strategy Enabled by Host–Defense–Peptides–Mimicking Synthetic Polypeptides, *Adv. Mater.*, 2020, **32**(36), 2001108.

49 H. Liu, W. Shen, W. Liu, Z. Yang, D. Yin and C. Xiao, From Oncolytic Peptides to Oncolytic Polymers: A New Paradigm for Oncotherapy, *Bioact. Mater.*, 2024, **31**, 206–230.

50 P. S. Stewart and J. William Costerton, Antibiotic, Resistance of Bacteria in Biofilms, *Lancet*, 2001, **358**(9276), 135–138.
51 P. Wan, W. Guo, Y. Wang, M. Deng, C. Xiao and X. Chen, Photosensitizer–Polypeptide Conjugate for Effective Elimination of Candida Albicans Biofilm, *Adv. Healthcare Mater.*, 2022, **11**(16), 2200268.
52 Y. Su, J. T. Yrastorza, M. Matis, J. Cusick, S. Zhao, G. Wang and J. Xie, Biofilms: Formation, Research Models, Potential Targets, and Methods for Prevention and Treatment, *Adv. Sci.*, 2022, **9**(29), 2203291.
53 Y. J. Zou, S. S. He and J. Z. Du, ε-Poly(L-lysine)-based Hydrogels with Fast-acting and Prolonged Antibacterial Activities, *Chin. J. Polym. Sci.*, 2018, **36**, 1239–1250.